

**SURGICAL ASPECTS, FINITE ELEMENT  
ANALYSIS AND X-RAY CORRELATION OF  
FEMORAL NECK CHANGES IN THE  
OSTEOARTHRITIC HIP AFTER HIP  
RESURFACING SURGERY**

THIS IS A THESIS SUBMITTED IN FULFILMENT OF THE REQUIREMENTS FOR THE  
DEGREE OF DOCTOR OF PHILOSOPHY

BY

**Lawrence Kohan**

M.B., B.S., (Hons) (SydU), F.R.A.C.S.



UNIVERSITY OF TECHNOLOGY, SYDNEY

JULY 2010

© LAWRENCE KOHAN 2010

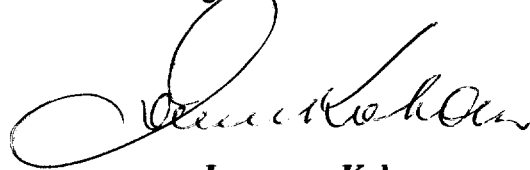
---

## **CERTIFICATE OF AUTHORSHIP/ORIGINALITY**

I certify that this thesis has not previously been submitted for a degree nor has it been submitted as part of the requirements for a degree except as fully acknowledged within the text.

I also certify that the thesis has been written by me. Any help that I have received in my research work and preparation of the thesis itself has been acknowledged. In addition, I certify that all information sources and literature used are indicated in the thesis.

Signature of Candidate

A handwritten signature in black ink, appearing to read 'Lawrence Kohan', written in a cursive style.

**Lawrence Kohan**

---

**To my parents.**

*“The more sand has escaped from the hourglass of our life, the  
clearer we should see through it.”*

Niccolo Machiavelli (1469–1527) Florentine philosopher, writer and one of the  
founders of modern political science

## ACKNOWLEDGEMENTS

This has been a long project, and would not have been possible to proceed to completion without the encouragement and support, patience and tolerance of Prof. Bessim Ben Nissan. I am very grateful for his help. I am also very grateful to Dr Mark Gillies, without whose help, as well, this project would not have been possible. His expertise in finite element analysis, computer programming and assessment was invaluable.

However, none of this would have been possible without the indulgence and tolerance of my family, who understood why their husband and father was not there.

My gratitude to you all.

## **ABSTRACT**

### **Background:**

Hip resurfacing is a logical choice for the treatment of symptomatic osteoarthritis as the degenerative process affects primarily the articular surface. It has been tried previously but failed. Recent improvements in metallurgy, manufacture and engineering have resulted in the development of a new series of implants which appear to be much more successful. Over the last 10 years, they have been used with enthusiasm and increasing popularity. However, over the last two years or so, their popularity has diminished with an awareness of significant complications developing. The complications relate primarily to early fracture, and the possible development of adverse reactions to metal ions. Component position may be implicated in the development of these complications.

### **Aims:**

1. To examine x-rays post-operatively of patients who have had hip resurfacing surgery and determine whether bone remodelling has occurred
2. If it has occurred, whether it is consistent with the changes predicted by the loading redistribution by the finite element stress analysis.
3. The use of finite element analysis to measure the effects of surgical technique and some of the factors related to femoral component positions on the bone stress distribution and morphological changes over time.

4. Improvements and suggestions regarding surgical aspects, (alterations in the valgus and varus alignment, the effect of anti-version and retro-version of the femoral component, the effect of incomplete seating of the femoral component and the effect of the cement mantle thickness) and to address concerns in relation to hip resurfacing surgery.

### **Materials and Methods:**

For the x-ray analysis 89 patients with 90 resurfacings were present in our database. The Birmingham (Smith and Nephew) hip resurfacing was used in all patients. There were 68 men and 22 women, with a mean age of 52 years. All patients had the underlying diagnosis of osteoarthritis. 33 patients agreed to be part of the study and were available for evaluation. These patients had x-rays, which were accurate enough to determine the measurements. Standardized AP x-rays were obtained so that the femoral neck could be measured in a reproducible way.

For the finite element analysis, a three-dimensional mesh was created using ten node tetrahedral elements. The bone contours on which the mesh was based on were extracted from CT scans. The material properties derived from the CT scans were applied locally. Muscle forces were applied as at heel strike, during normal gait. Two models were created, a reference or preoperative model and a treated, post-operative model. The integration points served as sensors. Both models were loaded identically over a period of 48 virtual months and the changes between the reference and the treated models assessed. Bone mass gain or loss was assessed as

well as the region of the femoral head and neck where the change occurred, determined. The effect of alterations in the valgus and varus alignment, the effect of anti-version and retro-version of the femoral component, the effect of incomplete seating of the femoral component and the effect of the cement mantle thickness were variables which were examined.

### **Results:**

Alterations in bone mineral density developed quickly after implantation and appeared to be stabilised within 12 months. Under the femoral component superiorly, bone loss occurs. In other areas, generally, an increase in bone density is seen. Maximum bone loss under the femoral head was approximately 85%, and maximum bone in gain at the base of the femoral neck inferiorly was 60%. The optimal valgus alignment was close to neutral in the femoral neck and highly valgus and varus alignments led to the development of bone loss. In relation to the version of the femoral stem within the neck, slight anteversion, 5°, as opposed to retroversion was favourable. Incomplete femoral component seating lead to significant alterations in tensile strain and potential displacement. Both displacement and strain rose dramatically beyond 3 mm of incomplete seating. The cement mantle thickness modelling was inconclusive as to its effect but it was noted that the most dramatic bone mass loss was with the cementless implant.

In the x-ray analysis we found that immediately under the femoral component, the femoral neck diameter diminished by 3.52% ( $p=0.001$ ). Distally, the neck

increased in diameter by 3.13% ( $p = 0.011$ ). On the control side, no significant change in the neck width was observed.

An increase in the body mass index produced increasing widening at the base of the femoral neck but the neck narrowing under the femoral component was not affected by BMI.

We did not see an influence of age on the changes in femoral neck width in the resurfacing patients.

**Conclusion:**

There is change in the femoral neck morphology after hip resurfacing surgery. Finite element analysis has predicted that this would occur as a result of changed loading patterns. The location and type of remodelling that has occurred, was also predicted by the finite element analysis. The change in neck width appears to be a manifestation of remodelling of bone in response to these altered loading patterns.

It was clearly established that surgical techniques such as a slightly valgus component alignment, with a neutral or slightly anteverted stem, induced changes. Remodelling was seen on follow-up x-rays. A cemented and fully seated femoral component is the optimal alignment. In the proximal part, stress shielding occurs, while distally, where the stress shielding was less, the effect of body weight on the remodelling was more pronounced.



# TABLE OF CONTENTS

<b>CERTIFICATE OF AUTHORSHIP/ORIGINALITY</b>	<b>II</b>
<b>ACKNOWLEDGEMENTS</b>	<b>IV</b>
<b>ABSTRACT</b>	<b>V</b>
<b>TABLE OF CONTENTS</b>	<b>IX</b>
<b>ABBREVIATIONS</b>	<b>XIV</b>
<b>LIST OF PUBLICATIONS</b>	<b>XV</b>
<b>CONFERENCE PROCEEDINGS</b>	<b>XVII</b>
<b>LIST OF FIGURES</b>	<b>XIX</b>
<b>LIST OF TABLES</b>	<b>XXVIII</b>
<b>1 Introduction</b>	<b>1</b>
<b>1.1 Background</b>	<b>2</b>
<b>1.2 Aims</b>	<b>4</b>
<b>1.3 Thesis Outline</b>	<b>5</b>
<b>2 Literature Review</b>	<b>7</b>
<b>2.1 Anatomy</b>	<b>8</b>
2.1.1 Osteology	8
2.1.2 Acetabulum	11
2.1.3 Femur	11
2.1.3.1 Head	13
2.1.3.2 Neck	14
2.1.4 Greater trochanter	18
2.1.5 Lesser trochanter	18
2.1.6 The shaft	19
2.1.7 Capsule and ligaments	19
2.1.7.1 The fibrous capsule	20
2.1.7.2 The iliofemoral ligament	22
2.1.7.3 The pubofemoral ligament	22
2.1.8 The ischiofemoral ligament	22
2.1.8.1 The ligament of the head of the femur	23
2.1.8.2 The acetabular labrum	23
2.1.8.3 The transverse ligament of the acetabulum	23

2.1.9	Vascular supply	24
2.1.9.1	Arterial supply	24
2.1.9.2	Venous drainage	34
2.1.10	Muscles	35
2.1.10.1	The flexors and extensors	36
2.1.10.2	The iliopsoas	36
2.1.10.3	Rectus femoris	37
2.1.10.4	Gluteus maximus	37
2.1.10.5	The hamstrings	38
2.1.10.6	Adductors and abductors	38
2.1.10.7	Gluteus medius	38
2.1.10.8	Gluteus minimus	39
2.1.10.9	Adductor longus	39
2.1.10.10	Adductor brevis	39
2.1.10.11	Adductor magnus	40
2.1.10.12	Gracilis	40
2.1.10.13	Pectineus	40
2.1.11	The rotators	40
2.1.11.1	Tensor fascia lata	41
2.1.11.2	Obturator internus	41
2.1.11.3	The gemelli	41
2.1.11.4	Pyriformis	42
2.1.11.5	Quadratus femoris	42
2.1.12	Embryology	42
2.1.12.1	Ossification	44
2.1.12.2	Nerve supply	46
<b>2.2</b>	<b>Hip Biomechanics</b>	<b>49</b>
2.2.1	Definition of the hip	49
2.2.2	Function of the hip joint	50
2.2.3	Motion of the hip joint	50
2.2.3.1	Degrees of freedom	51
2.2.4	Forces	52
2.2.4.1	External forces	53
2.2.4.2	Internal forces	55
2.2.5	Hip joint reaction calculations	60
2.2.6	Biomechanical simulations	63
2.2.6.1	Physiological loading simulations	63
<b>2.3</b>	<b>Bone – Structure and Function</b>	<b>76</b>
2.3.1	Macroscopic bone structure	76

2.3.1.1	Neurovascular supply	78
2.3.1.2	Woven bone tissue	79
2.3.1.3	Trabecular bone structure	79
2.3.1.4	Cortical lamellar bone	80
2.3.2	Microscopic structure	81
2.3.2.1	Extracellular matrix	81
2.3.3	Cellular elements	87
2.3.3.1	Osteoblasts	87
2.3.3.2	Bone lining cells	88
2.3.3.3	Osteocyte	89
2.3.3.4	Osteoclasts	91
2.3.4	Bone remodelling	93
2.3.4.1	The remodelling cycle	94
2.3.4.2	Control of remodelling	97
2.3.5	Mechanical regulation of structure	99
2.3.6	Mechanical environment	102
2.3.7	Proposed mechanisms for bone remodelling	107
2.3.7.1	Descriptive model	108
2.3.7.2	Equilibrium models	108
2.3.7.3	Optimisation models	113
2.3.8	The cellular environment	117
2.3.9	Mechanical properties of bone	117
2.3.9.1	Cortical bone	118
2.3.9.2	Trabecular bone	119
<b>2.4</b>	<b>Osteoarthritis</b>	<b>120</b>
2.4.1	Incidence	121
2.4.2	Aetiology	123
2.4.3	Pathology	126
2.4.3.1	Macroscopic	126
2.4.3.2	Microscopic	129
2.4.4	Radiology	131
2.4.5	Treatment	131
2.4.5.1	Medical	133
2.4.5.2	Surgical	134
2.4.5.3	Biological treatment	136
<b>2.5</b>	<b>Total Hip Replacement</b>	<b>137</b>
2.5.1	Prosthetic factors	138
2.5.1.1	Cemented prostheses	138
2.5.1.2	Uncemented hip replacements	146

2.5.1.3	Modularity	150
2.5.1.4	Bearing surfaces	151
2.5.1.5	Bone conserving femoral implants	153
2.5.1.6	The thrust plate prosthesis (Zimmer)	156
2.5.1.7	Mayo conservative hip (Zimmer)	156
2.5.1.8	The cut prosthesis (Eska)	157
2.5.2	Acetabular component	162
2.5.3	Outcomes of total hip replacement	165
2.5.4	Hip Resurfacing Arthroplasty	168
2.5.4.1	History	168
2.5.5	The birmingham hip resurfacing prosthesis	177
2.5.5.1	Metallurgy and manufacture	177
2.5.5.2	Metallic components of the prostheses	182
2.5.5.3	Surgical technique	184
2.5.5.4	Results of hip resurfacing	195
2.5.5.5	Problems associated with hip resurfacing	200
<b>3</b>	<b>Methodology</b>	<b>205</b>
3.1	Introduction	206
3.2	Computer Modelling	209
3.2.1	Model generation	209
3.2.2	Finite element model application	222
3.2.2.1	Case description	222
3.2.2.2	Analysis	223
3.2.2.3	Boundary conditions	227
3.2.2.4	Material properties	228
3.2.3	Variables	229
3.2.3.1	Alignment in the sagittal plane	229
3.2.3.2	Alignment in the coronal plane (anteversion/retroversion)	231
3.2.3.3	The effect of incomplete seating of the femoral component	232
3.2.3.4	The effect of altering the cement mantle thicknesses	233
3.2.3.5	The effect of cement-filled voids in the femoral head	234
3.3	Analysis of Radiographs	235
<b>4</b>	<b>Results</b>	<b>245</b>
4.1	Finite Element Results	246
4.1.1	Presentation of results	246
4.1.1.1	Bone mineral density plots	248

4.1.1.2	Varus/valgus bone mass change time history plots - bone mass change time history plots	254
4.1.1.3	Anteversion / retroversion alignment	259
4.1.2	Implant head offset	264
4.1.3	Physical displacement and changes in tensile strain	274
4.1.4	X-ray correlation	277
4.1.5	Cement mantle thickness	281
4.1.6	Bone mass change equilibrium plots	286
<b>4.2</b>	<b>B. Results of x-ray Examination in Relation to Neck Width Measurements</b>	<b>288</b>
4.2.1	Time effects	288
4.2.2	Influence of body mass index	292
4.2.3	Influence of age	293
<b>5</b>	<b>Discussion</b>	<b>295</b>
<b>5.1</b>	<b>Changes in Bone Mineral Density</b>	<b>296</b>
5.1.1	Effect of varus / valgus alignment	300
5.1.2	Effect of anteverted and retroverted alignment	305
5.1.3	Effect of implant offsets	309
5.1.4	Effect of cement mantle thickness	316
<b>5.2</b>	<b>Radiological Evaluation</b>	<b>319</b>
<b>6</b>	<b>Conclusion</b>	<b>327</b>
<b>7</b>	<b>References</b>	<b>331</b>

## **ABBREVIATIONS**

CT – Computer Tomography

MRI – Magnetic Resonance Imaging

FEA – Finite Element Analysis

CNC – Computer Numerically Controlled

CAD – Computer Aided Design

CAM – Computer Aided Manufacturing

DICOM - The Digital Imaging and Communications in Medicine

BHR – Birmingham Hip Resurfacing

C of G – Centre of gravity

DEXA – Dual-energy Xray Absorbtometry

VHD – Visual Human Data

HU – Hounsfield Unit

BMD – Bone Mineral Density

ROI – Region of Interest

BMI – Body Mass Index

## LIST OF PUBLICATIONS

GILLIES, R. M., HOGG, M. C., KOHAN, L. & CORDINGLEY, R. L. 2007. Adaptive bone remodelling of all polyethylene unicompartmental tibial bearings. *ANZ J Surg*, 77, 69-72.

GILLIES, R. M., KOHAN, L. & CORDINGLEY, R. 2007. Periprosthetic bone remodelling of a collum femoris preserving cementless titanium femoral hip replacement. *Comput Methods Biomech Biomed Engin*, 10, 97-102.

NIZAM, I., KOHAN, L. & KERR, D. 2007. Nocardia nova septic arthritis following total knee replacement: a case report. *J Orthop Surg (Hong Kong)*, 15, 390-2.

KERR, D. R. & KOHAN, L. 2008. Local infiltration analgesia: a technique for the control of acute postoperative pain following knee and hip surgery: a case study of 325 patients. *Acta Orthop*, 79, 174-83.

KERR, D. & KOHAN, L. 2009. Anaesthesia with Special Emphasis on Pain Control. In: MCMINN, D. (ed.) *Modern Hip Resurfacing*. London: Springer.

KERR, D. & KOHAN, L. 2009. Recovery and Rehabilitation. In: MCMINN, D. (ed.) *Modern Hip Resurfacing*. London: Springer.

NIZAM, I., KOHAN, L. & KERR, D. 2009. Hip resurfacing in an 88-year-old patient? Highlighting selection criteria for hip resurfacings in patients older than 65 years. *J Arthroplasty*, 24, 1143-1147.

CORDINGLEY, R., KOHAN, L. & BEN-NISSAN, B. 2010. What happens to femoral neck bone mineral density after hip resurfacing surgery? *Journal of Joint and Bone Surgery (UK)*, (in print).

CHOU, J., BEN-NISSAN, B., GREEN, D.W., VALENZUELA, S. M. & KOHAN L. 2010. Targeting and dissolution characteristics of bone forming and antibacterial drugs by harnessing the structure of micro-spherical shells from coral beach sand, *Adv. Eng. Mater.*, (in print).



## CONFERENCE PROCEEDINGS

- 2007      Orthopaedic Research Society, Annual Meeting, San Diego, USA, February 2007 Adaptive bone remodelling of the Birmingham of hip resurfacing and Cormet Components – Poster. Impaction loads during insertion of hip resurfacing components – poster. Birmingham hip resurfacing implant surgical orientation influence on adaptive bone remodelling – Poster
- 2007      Institution of Mechanical Engineers, Engineers and Surgeons: Joined at the hip conference, London, England, April 2007 Monte Carlo Simulation of Biomechanics and Fracture Risk in Hip Resurfacing
- 2007      Australian Orthopaedic Association Annual Scientific Meeting, Gold Coast, Australia, October 2007 Birmingham Hip resurfacing in the over 65 age group – a case series of 114 patients. Impaction loads during the insertion of hip resurfacing components. What happens to femoral neck bone mineral density after hip resurfacing surgery?
- 2007      The Medlaw & AOA Medico Legal Society Clinical Conference, Sydney November 30 – December 2, 2007 Hip Resurfacing – an update

- 2008      Orthopaedic Research Society 54th annual meeting, San Francisco, March 2-5 “The influence of femoral hip resurfacing internal geometry on the loading of underlying bone – a finite element study.” Gillies R.M., Kohan L., Hogg M., Appleyard R.C. “Impaction loads during insertion of hip resurfacing implant: a finite element study” Hogg M. C., Kohan L., Appleyard R., Gillies R. M. “The effect of hip resurfacing acetabular version angle on ion level changes – a finite element study”
- 2008      European Orthopaedic Research Society, 17th Annual Meeting, Madrid, April 25 – 26 “Hip resurfacings in patients over 65 years of age? A single surgeon cases series of 111 Birmingham hip resurfacings in 105 patients” Nizam I., Kohan L., Kerr D.. “A case series of ninety nine hybrid metal-on-metal hips- Birmingham resurfacing cup and Birmingham modular head” Nizam I., Kohan L., Kerr D. “Do non-steroidal anti-inflammatory drugs cause endoprosthetic loosening?” Nizam I., Kohan L., Kerr D.
- 2008      Australian Orthopaedic Association Annual Scientific Meeting, Hobart, October 12 -16 “Laser guided component implantation” Kerr D., Kohan L. “Finite element analysis and surgical considerations of the impact of osteoporosis and osteoarthritis on hip resurfacing.” Kohan L., Brown T. “Metal on metal hip arthroplasty – Birmingham resurfacing cup and Birmingham modular head - a single surgeon series of 99 hip arthroplasties.” (Poster) Nizam I., Kohan L., Kerr D. “Do non-steroidal anti-inflammatory drugs cause endoprosthetic loosening?” (Poster) Nizam I., Kohan L., Kerr D.

## LIST OF FIGURES

Figure 2-1: Lower Limb, Anterior view (Grant, 1962).	9
Figure 2-2: Lower limb, Posterior view (Grant, 1962).	10
Figure 2-3: Detailed osteology of the proximal femur, showing points of muscle attachment (Bartleby.com, 1918).	13
Figure 2-4: The posterior aspect of the proximal end of the femur, impact, and split to show the underlying pattern of cancellous trabeculae (Garden, 1961).	15
Figure 2-5: X-ray showing pattern of trabeculae. L: lateral tension trabeculae M: medial compression trabeculae I: intertrochanteric arch W: Wards Triangle (Garden, 1961).	16
Figure 2-6: The posterior wall of the femoral neck is removed showing the thin wall, and the thick ridge of the protruding calca. LT: lesser trochanter F: calcar (Garden, 1961).	16
Figure 2-7: Bisected femur showing the extent of the calcar ridge (Garden, 1961).	17
Figure 2-8: X-rays in various degrees of rotation, showing the trabecular pattern of the femoral head and neck (Garden, 1961).	18
Figure 2-9: Hip Capsule – anterior (Davies, 1967).	20
Figure 2-10: Hip Capsule – posterior (Davies, 1967).	21
Figure 2-11: Anterior View a: medial femoral circumflex artery; e: lateral femoral circumflex artery; f: anterior cervical branch of the lateral femoral circumflex artery; g: anterior capital branch of the lateral femoral circumflex artery; h: trochanteric branch of the lateral femoral circumflex artery; j: branch of the lateral femoral circumflex artery near point of anastomosis with medial circumflex artery (Howe, 1950).	25
Figure 2-12: Angiographic study demonstrating that widespread perfusion of the femoral head provided by the medial femoral circumflex artery (Lavigne et al., 2005).	28
Figure 2-13: The perforation of the terminal branches of the medial femoral circumflex artery. 1. Head of the femur; 2 gluteus medius; 3 deep branch of the medial femoral circumflex artery; 4. The terminal sub synovial branches of the medial femoral circumflex artery. 5. Insertion and tendon of gluteus medius; 6. Insertion and tendon of piriformis. 7. The lesser trochanter with nutrient vessels. 8. The trochanteric branch. 9. The branch of the first perforating artery. 10. The trochanteric branches (Gautier et al., 2000).	28
Figure 2-14: Anterolateral view of the hip joint showing detail of vascular branches. e: lateral femoral circumflex artery; f: anterior cervical branch of lateral femoral circumflex artery; h: trochanteric branch of lateral femoral circumflex artery; j: anastomose in branch to medial femoral circumflex artery; l: trochanteric branches of superior gluteal artery (Howe, 1950).	30
Figure 2-15: Posterior view of hip joint showing detail of vascular supply a: medial femoral circumflex artery; c: posterior superior a capital branch of medial femoral circumflex artery; d: trochanteric branches of medial femoral circumflex artery ; m: inferior gluteal artery; p: trochanteric branches from first perforating artery; s: branch of the inferior gluteal artery to be	

external obturator foramen; u: branch of inferior gluteal artery to the internal obturator and gemelli muscles (Howe, 1950).	31
Figure 2-16: Acetabulum and the surrounding pelvic bone showing the attachment of muscles (Grant, 1962).	35
Figure 2-17: Upper end of the femur showing attachments of muscles (Grant, 1962).	36
Figure 2-18: A condensation of cells between the primitive femoral head and acetabulum indicate the formation of the future hip joint space (Watanabe, 1974). Arrow indicates demarcation at which the hip joint space will develop.	43
Figure 2-19: The early cartilage model of the acetabulum and femoral head at the age of eight weeks (Watanabe, 1974).	43
Figure 2-20: Ossification centres of the acetabulum (Bartleby.com, 1918).	45
Figure 2-21: Ossification centres of the femur (Bartleby.com, 1918).	46
Figure 2-22: Model of the leg (Luh et al., 1980).	52
Figure 2-23: Illustrates external forces applied to body normal ambulation.	54
Figure 2-24: Illustrates body mass caused by acceleration and deceleration (Charnley, 1968).	55
Figure 2-25: Time force curve of resultant hip force peaks during walking (Bergmann et al., 1993).	58
Figure 2-26: Illustrating reference frames associated with the "rigid bodies".	61
Figure 2-27: Illustrates femur model boundary conditions (Cristofolini, 1997).	69
Figure 2-28: Diagrammatic representation of a long bone (Answers.com, 2009)	77
Figure 2-29: Ultrastructure of compact bone and cancellous bone (SEER, 2009)	79
Figure 2-30: The seven stages of increasing complexity in organisation of the bone family of materials. Level 1: isolated crystals from human bone, and an unstained collagen fibril from turkey tendon. Level 2: electron micrograph graph of a mineralised collagen fibril from turkey tendon. Level 3: electron micrographs of a thin section of mineralised turkey tendon. Level 4: fibril array patterns of organisation found in the bone family of materials. Level 5: electron micrographs of a single osteon from human bone. Level 6: light micrographs of a fractured section through a fossilised human femur. Level 7: whole bovine bone (Weiner, 1998).	82
Figure 2-31: Plot of calcium content versus Young's modulus for a large variety of bones (Weiner, 1998).	84
Figure 2-32: Schematic representation showing (a) an arrangement of mineralised collagen fibrils alignment both with respect to crystal layers and fibril axes. This structure has orthotropic symmetry, (b) arrangement of mineralised collagen fibrils with only the fibril axes aligned. The structure has transverse isotropy (Weiner, 1998).	85
Figure 2-33: Four of the most common fibril array patterns of organisation. (a) Parallel fibrils. (b) Woven fibre structure. (c) Plywood like structure present in lamellar bone. (d) Radial fibril arrays (Weiner, 1998).	86
Figure 2-34: A bony trabeculum showing within the bone an osteocyte, and on the surface and osteoblast (utmb, 1998).	89

Figure 2-35: Osteocytes stained with RH 414 dye, show the widespread interlinkage network (Meyle, 2001).	92
Figure 2-36: Scanning electron micrograph showing osteoclast resorbing bone (Society, 2008).	95
Figure 2-37: Cycle of cancellous bone remodelling (Mosekilde, 1999).	96
Figure 2-38: Cortical bone remodelling, showing a cutting cone with leading osteoclasts followed by cuboidal osteoblasts in the channel. Villanueva Mineralized Bone Stain 100x (Villanueva, 2009).	97
Figure 2-39: A group of osteons, with the older, remodelled osteon fragments between the circular, new or osteons. Arrow points to an osteon remnant stop (Michigan).	97
Figure 2-40: Diagrammatic representation of the difference between modelling and Haversian remodelling. Modelling involves periosteal and endosteal activity, while Haversian remodelling with the production of secondary osteons, affects the porosity of the bone (Pearson and Lieberman, 2004).	98
Figure 2-41: Responses of bone to loading.	102
Figure 2-42: Diagram A shows a simple stress strain curve, identifying the linear relationship portion, for which Young's modulus can be calculated, and the area where the linear relationship breaks down.. Diagram B shows the influence of cyclic frequency on the stress strained relationship, demonstrating increase in stiffness with increase in cycles (Pearson and Lieberman, 2004).	103
Figure 2-43: Conceptual representation of mechanostat function. The bone, at the top right of the figure, represents the anatomical shape. The box below the bone represents the interior of the bone with the various factors influencing remodelling, either internal or surface (Frost, 1987).	111
Figure 2-45: The stress-strain behaviour of cortical and trabecular bone is shown for different densities (Miller et al., 2007).	120
Figure 2-46: Incidence of osteoarthritis of the hand, hip, and knee (Oliveria et al., 1995).	122
Figure 2-47: Risk factors in the pathogenesis of osteoarthritis (Felson et al., 2000).	123
Figure 2-48: Diagrammatic representation, of the interplay of multiple substances at the molecular level, which mediate the development and progression of osteoarthritic degeneration. In the diagram, cytokines, growth factors, proteases, and inflammatory mediators are shown, as a theoretical mechanism for the development of osteoarthritis.	125
Figure 2-49: Diagrammatic representation of the changes occurring in an osteoarthritic joint, as compared to normal (Smith et al., 2000).	127
Figure 2-50: Femoral head removed it surgery, for osteoarthritis. It shows full thickness articular cartilage loss, eburnated bone, and osteophyte formation.	127
Figure 2-51: The relationship between bone loading and remodelling. This is Bombelli's concept of how hip joint deformities associated with osteoarthritis develop in relation to abnormal loads. The bottom diagram a shows a femoral neck fracture. Diagram b is a normal hip configuration. Diagram c represents early arthritic changes, which have progressed in d and are very severe in e. The shaded area represents a "normal" region in which bone apposition and bone removal are balanced (Bombelli, 1979).	129

Figure 2-52: Normal and osteoarthritic articular cartilage. The loss of the surface layer is visible, together with disorganisation of the cellular structure. H & E Stain (Abramson, 2007). The features of normal cartilage are contrasted with those of osteoarthritic cartilage. Of note is the breakdown of the superficial layers of the articular cartilage, with clefts extending into the middle zone. The staining is different, indicating loss of mucopolysaccharide. Increased cellularity is also present in the osteoarthritic cartilage, with clusters of cells being noted. The overall thickness of the cartilage is reduced.	130
Figure 2-53: X-rays of normal and osteoarthritic hips identifying the changes characteristic of osteoarthritis (arrow –denser bone and no gap between head and acetabulum).	131
Figure 2-54: The preoperative and post-operative x-rays are shown. In the post-operative x-ray the appearance of a joint space is noted where bone on bone contact was present (arrow).	135
Figure 2-55: Themistocles Gluck (Eynon-Lewis et al., 1992).	139
Figure 2-56: Acetabular cup of the Smith- Peterson type (Museum).	140
Figure 2-57: Smith-Peterson cup in place (Gmbh, 2006).	141
Figure 2-58: Charnley total hip replacement prosthesis (Charnley, 1972).	141
Figure 2-59: X-ray of Cemented Charnley total hip replacement in place (Charnley, 1972).	142
Figure 2-60: Clean air enclosure, with special air conditioning and airflow, at the Wrightington hospital, where Sir John Charnley operated (Charnley, 1972).	143
Figure 2-61: Exeter implant (Stryker) of the taper-slip design, with an x-ray showing the implant in place. <a href="http://www.bonedoctor.com.au/exerter-stem.html">http://www.bonedoctor.com.au/exerter-stem.html</a> .	144
Figure 2-62: Spectron stem (Smith and nephew), an example of the composite beam type of cemented steam prosthesis. (Surgical guide for Spectron total hip replacement – Smith and Nephew, Memphis, Tennessee, USA).	145
Figure 2-63: Cumulative percent revision of primary conventional total hip replacement by fixation (Association, 2008).	150
Figure 2-64: Birmingham mid-head resection prosthesis.	155
Figure 2-66: X-ray of a patient with a thrust plate prosthesis in place.	156
Figure 2-67: X-Ray of Mayo short stem prosthesis (Kluge, 2008).	157
Figure 2-68: Photograph and x-ray of the Cut prosthesis in place (Decking et al., 2008).	158
Figure 2-69: X-rays of the Proxima prosthesis (left). An image of the prosthesis (right). ( <a href="http://www.hipsforyou.com/proximahip.php">www.hipsforyou.com/proximahip.php</a> ).	159
Figure 2-70: The Silent hip x-ray.	160
Figure 2-71: Product information on the Chendo prosthesis (provided by the patient), showing a diagrammatic representation of the prosthesis.	161
Figure 2-72: X-rays of the Chendo prosthesis, at approximately 40 years of follow-up.	162
Figure 2-73: The Mechanism of Late Aseptic Loosening of Cemented Acetabular Components. (A) Bone resorption and membrane formation is initiated circumferentially at the intra-articular margin of the implant. Bone resorption and membrane formation then progresses, in a three-dimensional manner, toward the dome of the implant. (B) Microscopic evaluation of the transition zone from an area with membrane interposition between cement and bone to an area of intimate cement-bone	

contact was characterised by a cutting wedge of bone resorption. The hallmark of this region is extracellular and intracellular polyethylene particles in macrophages, with active bone resorption by macrophages. This process is fuelled by small particles of polyethylene wear debris migrating along the cement-bone interface (Schmalzried et al., 1992).	163
Figure 2-74: Cross-section view of a third-generation modular uncemented acetabular prosthesis with a polyethylene bearing, demonstrating the features which are currently believed to be associated with the best results. The bearing surface is not elevated above the rim. The locking mechanism, arrows, is recessed into the interior of the shell to minimise the stresses (R3 SMITH AND NEPHEW) (Ries, 2008).	165
Figure 2-76: Shows the cumulative percentage revision of primary total hip replacements for females by age, and figure shows the same for men.	167
Figure 2-77: Smith-Petersen Vitallium hemiarthroplasty (Grigoris et al., 2006).	170
Figure 2-79: Charnley Teflon total hip resurfacing (Grigoris et al., 2006).	171
Figure 2-80: Townley hip resurfacing (Grigoris et al., 2006).	172
Figure 2-81: Muller hip resurfacing (Grigoris et al., 2006).	173
Figure 2-82: Paltrinieri hip resurfacing (Grigoris et al., 2006).	173
Figure 2-83: Freeman hip resurfacing (Grigoris et al., 2006).	174
Figure 2-84: Wagner metal on polyethylene resurfacing (Grigoris et al., 2006).	174
Figure 2-85: Wagner metal on metal resurfacing (Grigoris et al., 2006).	175
Figure 2-86: Amstutz cementless hip resurfacing (Amstutz et al., 1978).	175
Figure 2-87: Birmingham hip resurfacing prosthesis. (Illustration provided by Smith & Nephew – Memphis, Tennessee)	177
Figure 2-88: Wax moulds are assembled on to a “tree”, multiple moulds together. . (Illustration provided by Smith & Nephew – Memphis, Tennessee)	178
Figure 2-89: The wax moulds are covered in ceramic and baked to remove the wax. (Illustration provided by Smith & Nephew – Memphis, Tennessee)	179
Figure 2-90: The ceramic is then a negative imprint of the final prosthesis. (Illustration provided by Smith & Nephew – Memphis, Tennessee)	179
Figure 2-91: The ceramic moulds are filled with molten metal, and then the ceramic external shell removed. . (Illustration provided by Smith & Nephew – Memphis, Tennessee)	180
Figure 2-92: Honing and polishing. (Illustration provided by Smith & Nephew – Memphis, Tennessee)	181
Figure 2-93: Final product ready for sterilization. (Illustration provided by Smith & Nephew – Memphis, Tennessee)	182
Figure 2-94: In the templating process, the anticipated position of the femoral component is determined, and measured (McMinn, 2007).	185
Figure 2-95: The aim of the templating process is demonstrated. With the templating, the alignment of the femoral component can be anticipated with a fair degree of accuracy. a) neutral alignment. b) varus alignment. c) marked valgus alignment with risk of notching.	186
Figure 2-96: Positioning of guide pin, and femoral cutting guide (McMinn, 2007).	189

Figure 2-97: The femoral head and the jig are connected. The jig is used to determine angle of component placement and to ensure that notching will not occur.	190
Figure 2-98: Head preparation proceeds. The barrel reamer is used to prepare the femoral head.	191
Figure 2-99: The steps involved in preparation of the femoral head (McMinn, 2007).	192
Figure 2-100: Femoral component filled with cement in preparation for impaction into position.	193
Figure 2-101: Impaction of the femoral component at surgery.	193
Figure 2-102: Sequence of steps from the initial osteoarthritic head, to the resurfaced head.	194
Figure 2-103: Taken from the 2009 edition of the Australian joint registry report, the cumulative percentage revision of primary conventional total hip replacement and total resurfacing replacement, excluding infection, is shown (Association, 2009).	199
Figure 2-104: The risk within six years, of sustaining a femoral neck fracture, in women, with different bone mineral densities as assessed by DEXA (Nordin et al., 2008).	203
Figure 3-1: (a) Intact in bone geometry (b) Reconstructed bone geometry	210
Figure 3-2: Finite element mesh for (a) the intact model and (b) the reconstructed model.	211
Figure 3-3: The fixed base is shown. The hip joint contact force is applied to the (a) intact model and the (b) reconstructed femur model with the femoral component in place is shown.	213
Figure 3-4: Muscle forces applied to the femur. As described by Duda, all thigh muscles, abductors, adductors, and iliotibial band were included in the modelling (Duda et al., 1998).	214
Figure 3-5: The gait cycle, with the arrow indicating the 45% point, at heel strike, where the measurements are made for the analysis (Goodship, 1992).	216
Figure 3-6: CT (left) converted to mapped material properties (right).	217
Figure 3-7: Bone remodelling stimulus. The current mechanical signal as shown in this example (blue arrow), will result in the decrease in bone density proportional to the error signal. In this instance the proportionality factor is the slope of the resorption curve.	218
Figure 3-8: Cross-Sections of the Femoral Component- femoral head composite, arrows showing variability in the cement layer.	219
Figure 3-9: Flow chart demonstrating the adaptive bone remodelling algorithm.	221
Figure 3-10: The regions of interest in the femoral neck analysed for changes in the bone mineral density.	221
Figure 3-11: Computer model of the Birmingham hip resurfacing component and the real component.	223
Figure 3-12: Virtual femur with the virtual prosthesis in place.	224
Figure 3-13: The geometry of the reconstructed femur is shown, with a reference model, and a varus alignment model in 28.5° of varus tilt away from the reference case.	230
Figure 3-14: Geometry of reconstructed femurs showing reference model (5.0 degrees varus rotation case), 5.0 degrees anteversion case (green) and 5.0 degrees retroversion (blue).	232
Figure 3-15: Geometry of reconstructed femurs showing reference model (0mm offset) and the 5mm offset case. Other offset cases lie intermediate to these two cases.	233



Figure 3-16: Variation in cement mantle thickness included a (a) 0mm cement mantle, (b) 1 mm cement mantle, (c) 3 mm cement mantle and (d) 5 mm cement mantle. _____	234
Figure 3-17: Age and gender distribution of the patients whose x-rays were evaluated. The total group of patients is shown in the light pink and light blue columns for women and men respectively. The subgroup studied, the patients who were able to be followed up, is shown in the dark red and dark blue columns for women and men respectively. _____	237
Figure 3-18: Body mass index and ages of the patients whose x-rays were evaluated. The light green bars refer to the total group of patients surveyed, and a dark green referred to the responders, the patients whose x-ray data was available for study. _____	238
Figure 3-19: Breakdown of component sizes used in the operations evaluated. _____	239
Figure 3-20: Method of calculation of inferior make width. _____	240
Figure 3-21: Femoral neck axis established on the control side. _____	243
Figure 3-22: Measurement of neck width on the control side. The point on the lesser trochanter of the non-operated side, used as a reference point is shown. _____	244
Figure 4-1: Virtual x-ray showing nine regions of interests (ROIs) around the stem used to calculate the change in bone mineral density. The mesial head of the prosthesis is not shown for ease of observation. _____	249
Figure 4-2: BMD changes at reference angle (stem is positioned 18.5 degrees valgus rotation from the centre of the neck of the femur). ROI refers to "region of interest" as indicated in Figure 4-1. _____	250
Figure 4-3: BMD changes at 5 ° varus from the reference angle. _____	250
Figure 4-4: BMD changes at 10 ° varus from the reference angle. _____	251
Figure 4-5: BMD changes at 13.5 ° varus from the reference angle. _____	251
Figure 4-6: BMD changes at 18.5 ° varus from the reference angle. _____	252
Figure 4-7: BMD changes at 23.5 ° varus from the reference angle. _____	252
Figure 4-8: BMD changes at 28.5 ° varus from the reference angle. _____	253
Figure 4-9: Graph of bone mass gain for different varus /valgus alignments. _____	255
Figure 4-10: Graph of bone mass loss for different varus / valgus alignments. _____	256
Figure 4-11: Summary of BMD change per zone at 12 months. _____	258
Figure 4-12: BMD changes at neutral position (5.0 ° varus case). _____	260
Figure 4-13: BMD changes for implant at 5 ° anteversion. _____	260
Figure 4-14: BMD changes for implant at 5 ° retroversion. _____	261
Figure 4-15: Graph of bone mass gain for different torsion rotation. _____	261
Figure 4-16: Graph of bone mass loss for the different torsion rotation. _____	262
Figure 4-17: BMD changes at zero offset, component fully seated. _____	265
Figure 4-18: BMD changes at the 1 mm offset. _____	265
Figure 4-19: BMD changes at the 3mm offset. _____	266
Figure 4-20: BMD changes at 5 mm offset. _____	266
Figure 4-21: Graph of bone mass gain for various stem offsets. _____	267
Figure 4-22: Graph of bone mass loss for various stem offsets. _____	267

Figure 4-23: Compressive (Minimal Principal) stresses. Native hip. Units are in MegaPascals.	270
Figure 4-24: Stem in maximal valgus (reference case). The femoral component is fully seated for the initial case, and then progressively left unseated, 1 mm, 3 mm, and 5 mm, with progressively more cement at the proximal end of the femoral head, but the standard 1 mm of cement around the rest of the component. Scale is in megapascals. In this diagram of the most extreme case, the 5 mm offset configurations, the stresses within the extra thick cement mantle at the top of the femoral head can be seen.	271
Figure 4-25: Bone Resorption Signal (units in equivalent strain).	273
Figure 4-26: Bone Resorption Signal (units in equivalent strain).	273
Figure 4-27: Bone Deposition Signal for 1mm offset (units in equivalent strain).	274
Figure 4-28: Bone Deposition Signal for 5mm offset (units in equivalent strain).	274
Figure 4-29: System displacement for 1 mm offset. Scale is in millimetres of displacement.	275
Figure 4-31: Graphic representation in modelled femoral component displacement with varying degrees of offset of the femoral component (blue line and left hand scale). Changes in tensile strain are shown by the red line (right hand scale).	276
Figure 4-32: Well seated femoral component. There is minimal bony reaction. A minor degree of density increase at the base of the femoral stem is seen. Bony apposition to the stem is present without any lucent line.	278
Figure 4-33: Well seated femoral component. Bony reaction around the femoral stem tip is seen (arrows). This would indicate at least some degree of load shedding from the stem to the surrounding bone at this point. There is no evidence of lucency around the stem.	279
Figure 4-34: Radiolucent line around the femoral stem indicating possible increased mobility (arrows). On the inferior aspect, a lucent line is noted and on the superior aspect and area of sclerosis is present.	280
Figure 4-35: The femoral stem in a patient with avascular necrosis and loosening of the femoral component. Asymmetric lucency around the femoral stem is noted.	281
Figure 4-36: BMD changes for cementless implant.	283
Figure 4-37: BMD changes for 1 mm cement mantle thickness.	283
Figure 4-38: BMD changes for 3 mm cement mantle thickness.	284
Figure 4-39: BMD changes for 5 mm cement mantle thickness.	284
Figure 4-40: Graph of bone mass gain for various cement mantle thicknesses.	285
Figure 4-41: Graph of bone mass loss for various cement mantle thicknesses.	286
Figure 4-42: Change in mass bone density for each case. Bone deposition and bone loss are shown on the right and left of the vertical axis (Y axis) respectively.	287
Figure 4-43: This graph plots the percentage change in neck width at the superior and inferior measuring points for all the patients with a hip resurfacing prosthesis (red for the superior measuring point and blue for the inferior measuring point), and the control group of hips, the young operated hips in those patients who had had an operation on the contralateral side (Green).	289

Figure 4-44: Data points, showing the percentage change in neck width at those superior and inferior points for measurement on the operated side, and at the narrowest point of the femoral neck on the control side. Only the patients who had a control hip to be measured are shown in this graph. _____	290
Figure 4-45: The change in the width of the proximal femoral neck (blue dots) and the base of the neck (red dots) in relation to the BMI is shown. Correlation coefficient lines are shown. _____	292
Figure 4-46: The percentage change in neck diameter, superiorly (blue) and inferiorly (red), in relation to the age of the patient at the time of the initial operation. Correlation analysis is shown. There is no correlation with respect to age. _____	294
Figure 5-1: Biomechanical analysis of the loads across the weight-bearing hip. "R" is the resultant force across the hip joint, produced by the effects of gravity, and the counterbalancing force of the hip muscles (Pauwels, 1976). _____	302
Figure 5-2: Body weight resultant force, depicted on a cross-section of the hip, showing how the primary compression trabeculae are lined up along this vector (Garden, 1961). _____	302
Figure 5-3: From Freeman's article, (Freeman and Brown, 1978) showing his concept of optimal femoral component alignment. _____	303
Figure 5-4: Eska femoral component, with a modular stem left, and the Birmingham prosthesis, right. The stem can be removed completely on the Eska device or a short stem can be applied. The Birmingham has a solid, thicker and longer stem. _____	305

## LIST OF TABLES

Table 2-1: Internal muscle forces (Cristofolini, 1997).....	56
Table 2-2: Taken from Pearson (Pearson and Lieberman, 2004) describes the different proposed mechanisms, for bone remodelling. ....	115
Table 2-3: Revision rates of primary total resurfacing hip replacement (Association, 2008).....	196
Table 2-4: Hip surgery variables.....	197
Table 2-5: Analysis of revisions of total hip resurfacing procedures, using data from the Australian National joint replacement Registry, 2007. A breakdown by gender and age (M= Male and F= Female). ....	201
Table 3-1: Magnitude and direction of applied muscle forces.....	215
Table 3-2: Properties of bone, cement mantle, and the Birmingham resurfacing prosthesis (Huiskes and Verdonschot, 1997). ....	220
Table 4-1: A summary of the regions which gained, lost, or were unchanged, in relation to bone mineral density, when orientation of the femoral component was changed. The various areas are shown with bone deposition (Green), no change (yellow), and bone resorption (red) for the various alignment configurations of the femoral component. ....	257
Table 4-3: Summary of bone mineral density response.....	268